Author Manuscript

Author Manuscript

Author Manuscript

Author Manuscript

HHS Public Access

Author manuscript

Cell Rep. Author manuscript; available in PMC 2025 June 20.

Published in final edited form as:

Cell Rep. 2025 January 28; 44(1): 115183. doi:10.1016/j.celrep.2024.115183.

Deletion of AMP-activated protein kinase impairs metastasis and is rescued by ROS scavenging or ectopic CD36 expression

Gopalakrishnan Ramakrishnan[1], **Alexander R. Terry**[1,3], **Veronique Nogueira**[1], **Ahmed Magdy**[1], **Nissim Hay**[1,2,4,*]

[1]Department of Biochemistry and Molecular Genetics, College of Medicine, University of Illinois at Chicago, Chicago, IL 60607, USA

[2]Research and Development Section, Jesse Brown VA Medical Center, Chicago, IL 60612, USA

[3]Present address: Department of Radiation Oncology, Memorial Sloan Kettering Cancer Center, 1275 York Ave., New York, NY 10065, USA

[4]Lead contact

SUMMARY

AMPK's role in tumor initiation and progression is controversial. Here, we provide genetic evidence that AMPK is required for metastasis in mouse models of breast cancer. In a mouse model of spontaneous breast cancer metastasis, the deletion of AMPK before and after tumor onset decreased breast cancer metastasis, and similar results were obtained after AMPK deletion in breast cancer cell lines. The deletion of AMPK induces reactive oxygen species (ROS) levels *in vitro* and lipid oxidation *in vivo*, which likely impede metastasis. Indeed, antioxidants restore the ability of AMPK-deficient tumors to metastasize. By inhibiting acetyl-coenzyme A (CoA) carboxylases 1 and 2, AMPK maintains NADPH levels by reducing NADPH consumption in fatty acid synthesis and increasing NADPH generation via fatty acid oxidation, thus increasing the dependency on auxotrophic fatty acids. Consistently, AMPK is required for the expression of the fatty acid transporter CD36 in tumors, and ectopic expression of CD36 in AMPK-deficient cells restored their ability to metastasize.

In brief

Ramakrishnan et al. deleted AMPK in a spontaneous breast cancer metastasis mouse model and metastatic cell lines and showed that it is required for breast cancer metastasis. AMPK is required to mitigate ROS levels by generating NADPH, and thus, antioxidants could restore metastasis in AMPK-deficient cells.

Graphical Abstract

This is an open access article under the CC BY-NC-ND license (http://creativecommons.org/licenses/by-nc-nd/4.0/).

*Correspondence: nhay@uic.edu.

AUTHOR CONTRIBUTIONS

G.R. generated all the animals and cell lines for this work with the help of A.R.T. and A.M. G.R. performed most of the experiments. V.N. generated parts of the images in Figure 4. G.R., A.R.T., and N.H. wrote the manuscript. N.H. supervised the project.

DECLARATION OF INTERESTS

The authors declare no competing interests.

Author Manuscript Author Manuscript Author Manuscript Author Manuscript

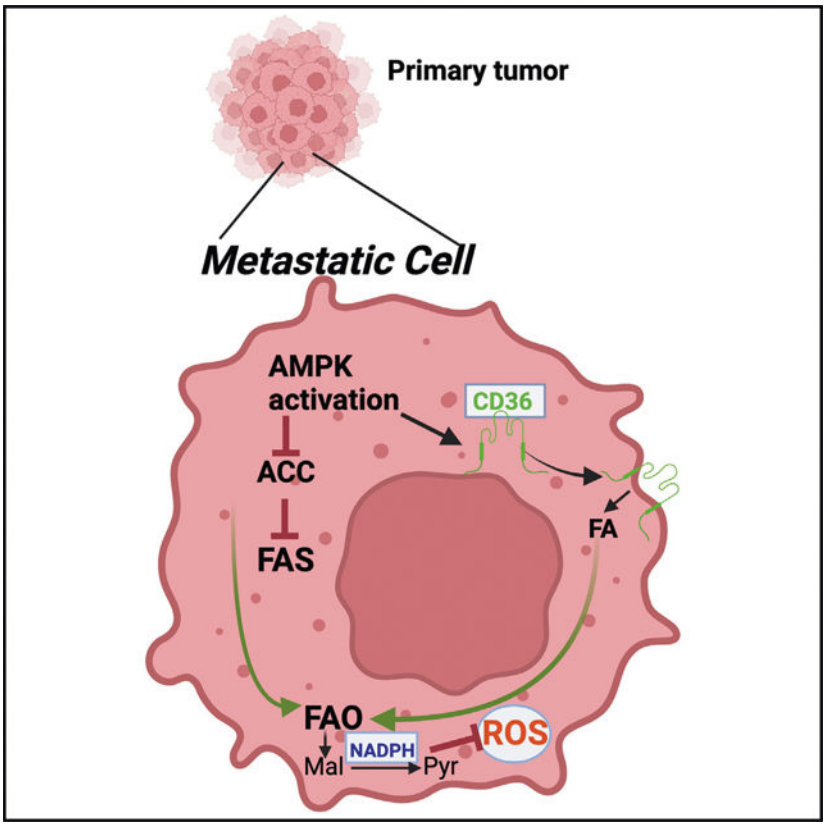

INTRODUCTION

Mortality from cancer primarily occurs due to metastasis via dissemination and colonization of the cancer cells in distant organs. During invasion, cancer cells show an altered and decreased cell-matrix interaction, and this interaction is further reduced in the circulation. An inevitable outcome of matrix detachment is reactive oxygen species (ROS) accumulation.[1] Indeed, it was demonstrated that high ROS levels impede migration and invasion *in vitro* and metastasis *in vivo*.[2,3] Cancer cells combat excessive ROS by scavenging it via NADPH, which is generated primarily by the oxidative pentose phosphate pathway (PPP) but can also be generated in the cytoplasm by malic enzyme 1 (ME1) and isocitrate dehydrogenase 1 (IDH1) and, to some extent, by the folate pathway.[4–6] During matrix detachment, cells have a diminished ability to take up glucose.[7] Impaired glucose uptake results in a reduction in ATP turnover due to reduced glycolysis and glucose shuttling into the PPP, which is also the primary source for NADPH generation.[1,7] NADPH is crucial for the proper functioning of the antioxidant defense mechanisms by recycling the oxidized glutathione peroxidases (GPXs) and peroxiredoxins (PRXs) in the cells.

AMP-activated protein kinase (AMPK) plays a pivotal role in maintaining ATP homeostasis. However, we showed that AMPK also plays a critical role in NADPH homeostasis under energy stress conditions.[1] AMPK activation during energy stress, such as glucose deprivation, prolongs cell survival via redox regulation. Under these conditions, NADPH generation by the PPP is impaired, but AMPK induces alternate routes to maintain NADPH

Author Manuscript Author Manuscript Author Manuscript Author Manuscript

levels and inhibit cell death. Interestingly, during matrix detachment, cells markedly decrease glucose uptake by up to 80% despite glucose availability.[1,8] Therefore, when cancer cells migrate to the lumen during solid tumor formation, they no longer consume glucose and undergo energetic stress.[7] This energetic stress is derived from a decrease in ATP production, but more importantly, a decline in NADPH levels that leads to elevation of intracellular ROS levels.

When AMPK is activated, it phosphorylates and inhibits the activities of acetyl-coenzyme A (CoA) carboxylases 1 and 2 (ACC1 and ACC2), which are required for fatty acid synthesis (FAS) and the inhibition of fatty acid oxidation (FAO), respectively. The inhibition of ACC1 and ACC2 by AMPK maintains NADPH levels by reducing NADPH consumption in FAS and increasing NADPH generation via FAO. The inhibition of mitochondrial-associated ACC2 by AMPK decreases localized malonyl-CoA that otherwise inhibits the carnitine palmitoyl transferase 1 (CPT1), which mediates the rate-limiting step in FAO and is responsible for acyl-carnitine transport into the mitochondria. By promoting FAO, AMPK provides acetyl-CoA to drive the TCA cycle, thereby increasing the transport of malate and citrate to the cytosol, the flux from malate to pyruvate by ME1, and the conversion of isocitrate to αKG by IDH1, both of which generate NADPH. Thus, AMPK, in addition to its role in ATP homeostasis, plays a key role in NADPH maintenance. This activity of AMPK is critical for cancer cell survival under energy stress conditions, such as glucose limitations, anchorage-independent growth, and solid tumor formation *in vivo*.[1]

Following our initial observation that AMPK is pro-tumorigenic,[1] others have shown that AMPK is required for tumorigenesis in leukemia and glioblastoma.[9,10] In a mouse model of nonsmall cell lung cancer (NSCLC) induced by p53 deletion and KRAS activation, it was shown that AMPK deletion inhibits, rather than promotes, tumorigenesis.[11] Moreover, higher levels of phosphorylated ACC1 (pACC1), an AMPK target, were shown to play a pro-metastatic role in breast and lung cancers,[12] and pACC1 levels were directly proportional to the node-positive status and worse overall survival in patients with head and neck squamous cell carcinoma (HNSCC) and breast cancer.[12,13] More recently it was shown that phosphorylation of pyruvate dehydrogenase alpha (PDHA) by AMPK is required for metastasis.[14] However, no genetic evidence in mouse models of metastasis was provided to show that AMPK is required for metastasis. Here, we show that both constitutive and conditional cell-autonomous deletions of AMPK in a transgenic MMTV-PyMT mouse model of breast cancer metastasis markedly impede metastasis. This reduction in metastasis is due to the elevated ROS levels, which are reversed by antioxidant treatment, catalase overexpression, or ACC1/2 ablation. Recently, we found that AMPK is required for the expression of CD36 (also known as fatty acid translocase).[15] CD36 is a plasma membrane protein that is required for the uptake of fatty acids and metastasis in models of breast cancer, HNSCC, and melanoma.[15,16] We found that the deletion of AMPK, both in MMTV-PyMT mouse models and metastatic cell lines, decreased the expression of CD36 in tumors. Re-expression of CD36 in AMPK-deficient cells restored ROS neutralization, the NADP/NADPH ratio, FAO, and metastatic potential. Taken together, these findings assign a role to AMPK as a pro-metastatic entity that performs this function through ROS counterbalancing in cooperation with CD36.

Author Manuscript Author Manuscript Author Manuscript Author Manuscript

RESULTS

AMPK expression and activity are correlated with metastasis

Prior studies had demonstrated the importance of AMPK activity for cell survival during matrix detachment.[1] One obvious extrapolation of this phenomenon was the requirement for AMPK activity during metastasis, a process that requires cell detachment from the primary tumor to disseminate to the metastatic site.[17] We decided to obtain evidence for this conjecture and began by analyzing existing datasets for correlation between distant metastasis-free survival (DMFS) and AMPK expression. Intriguingly, we found a correlation between AMPK expression and metastasis, with a lower expression prognostic of longer DMFS in a breast cancer dataset[18] (Figure S1A). Since AMPK expression per se does not reflect its activity, we repeated the same analysis with a reverse-phase protein array (RPPA) dataset[19] to correlate pACC S79 levels with DMFS in breast cancer. ACC1/2 are both negatively regulated via phosphorylation by AMPK upon its activation, and hence their phosphorylated versions can serve as a useful measure of AMPK activity. As with AMPK expression, high pACC was associated with a higher incidence of distant metastasis (Figure S1B). To further validate our above observations, we stained a large breast cancer tissue microarray (TMA) containing normal tissues and tissues of different breast cancer stages, as well as metastatic lymph nodes, for pACC expression. Concordant with our dataset findings, the intensity of pACC staining increased with tumor stage and in metastatic lymph nodes, thereby indicative of increased AMPK activity (Figure S1C).

AMPK deletion markedly reduces metastasis and induces oxidative stress in mouse models of breast cancer metastasis

To determine if AMPK is required for metastasis, we chose the MMTV-PyMT mouse model wherein the polyoma virus middle T antigen expression in the mammary gland induces several signaling pathways that are altered in human breast cancer, including the SRC and PI3K pathways. Specifically, the MMTV-PyMT mouse model will result in the development of multifocal mammary adenocarcinomas, which closely resemble breast tumors in human, with a high incidence of metastatic lesions to the lymph nodes and lungs.[20] Our mouse studies were performed on two strains of the MMTV-PyMT models wherein mammarygland-specific ablation of AMPK could be performed either constitutively or in an inducible manner. The first strain carried a floxed version of α1 and α2 subunits of AMPK[21] along with MMTV-PyMT. Constitutive deletion in the mammary gland was achieved by crossing them with an MMTV-Cre strain to obtain either PM (*MMTV-PyMT; MMTV-Cre*) or PAM (*MMTV-PyMT; AMPKα1$^{f/f}$; AMPKα2$^{f/f}$; MMTV-Cre*) mice (Figure 1A).

To dissociate the effect of AMPK loss from normal mammary gland development, primary tumor growth, and metastasis, we generated a second novel transgenic mouse strain where the inducible deletion of AMPKα1 and α2 occurs due to a doxycycline (Dox)-infused diet or providing Dox in the water. A Cre recombinase inducible luciferase reporter was also introduced into the mice, thereby enabling us to track recombinase induction. The detailed schematic of the inducible deletion mechanism is shown in Figure 1F, and our final genotypes were named PL (*MMTV-PyMT; Tet(O)Cre; MMTV-rtTA; LSL.Luc*) and

Author Manuscript Author Manuscript Author Manuscript Author Manuscript

PAL (*MMTV-PyMT; AMPKα1$^{f/f}$; AMPKα2$^{f/f}$; Tet(O)Cre; MMTV-rtTA; LSL.Luc*) mice. Post-weaning, at tumor onset, both the PL and PAL mice were switched to Dox-water, and the recombinase induction was affirmed through luciferase expression in the mammary glands (Figure S2A). The stringent regulation of the recombinase expression was evident when selective luminescence signals were observed in the Dox-water-treated mice alone (Figure S2A).

At the experimental endpoint, when primary tumors reached the same size in all strains of mice to avoid the effect of primary tumor growth on metastasis, mice were euthanized and analyzed. Surprisingly, however, we did not observe a significant delay after deleting AMPK in reaching the endpoint as measured by Kaplan-Meir curves (Figures S2B and S2C). Although PAL mice reached the endpoint slightly later than PL mice, it was not statistically different (Figure S2C). The tumors were analyzed for the extent of AMPK deletion in the PM/PAM and PL/PAL (raised on Dox-water) cohorts. Western blotting for total levels of AMPKα revealed a marked reduction in its expression in both PAM and PAL mice compared to their respective controls (Figures 1B and 1G). In both mouse models, AMPK deletion significantly reduced lung metastases (Figures 1C and 1H). In addition, primary tumors were subjected to immunohistochemistry (IHC) for total AMPK and pACC and showed a marked difference among the PM/PL vs. PAM/PAL tumors (Figures 1D and 1I), which is also shown by immunoblotting for pACC (Figures 1E and 1J), therein providing further evidence of the efficiency of AMPK deletion. IHC staining was quantified using a previously published method by scoring the level of staining from 0 to 5.[22] We also analyzed primary tumor sections after AMPK loss by staining for 4-hydroxynonenal (4-HNE). 4-HNE is an α,β-unsaturated hydroxyalkenal that is produced by lipid peroxidation in cells. It is a stable product of lipid peroxidation that is produced in higher quantities during oxidative stress and is a useful readout for measuring ROS *in vivo*.[23] The intensity of 4-HNE staining was substantially higher in both PAM and PAL tumors compared to their respective controls (Figures 1D and 1I). Taken together, these results show that AMPK is required for metastasis even after tumor onset and suggest that AMPK deficiency increases oxidative stress, which could impede metastasis.

To further test the requirement for AMPK in metastasis, we knocked out AMPK in metastatic human (MDA-MB-231LM2 [231LM2] and MCF10CA1a) and mouse (E0771) breast cancer cell lines (Figure 2A). To confirm the efficacy of the knockout (KO), cells were treated with the AMPK activator A769662 (A76), and pACC levels were measured as a readout of AMPK activity (Figures S3A–S3C).

231LM2 wild-type (WT) and AMPK-KO cells were orthotopically implanted into the mammary fat pad of NSG mice. The cells also expressed a firefly luciferase reporter that enabled us to track dissemination and metastasis. At the endpoint, we quantified metastasis and found that AMPK ablation drastically reduced the incidence of metastasis to the lungs in all the experimental animals we analyzed (Figures 2B and 2C). Similar results were obtained when MCF10CA1a and E0771 cells were orthotopically implanted into NSG and C57BL/6 mice, respectively (Figures 2E and 2G).

Author Manuscript Author Manuscript Author Manuscript Author Manuscript

Primary tumor sections from all three orthotopic models were subjected to IHC for 4-HNE staining as a readout for oxidative stress. Increased 4-HNE was observed in the AMPK-null tumors derived from all three cell lines (Figures 2D–2F, 2H, S3D, and S3E). Thus, similar to MMTV-PyMT mice, AMPK is required for the metastasis of established cell lines, and AMPK deficiency is associated with increased oxidative stress in the primary tumors.

ROS neutralization overcomes the requirement of AMPK for metastasis

Our *in vivo* results suggest that AMPK-deficient tumors undergo increased oxidative stress. To test this *in vitro*, we grew cells on a low-attachment (poly(2-hydroxyethyl methacrylate) or poly-HEMA-coated) plates to mimic matrix detachment, and we found that AMPK activity is induced in the WT cells (Figures S4A–S4C). During matrix detachment, ROS levels and the NADP/NADPH ratio were significantly higher in the AMPK-KO cells when compared to the WT cells (Figures 4F, 4G, and S4D–S4G). These results are consistent with the role of AMPK activation promoting NADPH homeostasis to reduce ROS.

Next, we wanted to determine whether ROS scavenging could overcome the requirement of AMPK for *in vivo* metastasis. When drinking water was supplemented with NAC, we found that it markedly and significantly increased metastasis in PAM mice (Figure 3A). We next repeated the orthotopic xenograft experiments with 231LM2 WT and AMPK-KO cells, both in the presence and absence of NAC, and monitored its effect on metastasis. NAC was able to restore metastatic colonization in the absence of AMPK to a level higher than seen with the 231LM2 WT cells (Figures 3B and 3C). These results pointed toward ROS elevation impeding metastasis, particularly in the absence of AMPK. To further substantiate this view, we measured the extent of oxidative damage in the tumors derived from these animals by IHC for 4-HNE. The reduction in 4-HNE staining in NAC-treated AMPK-KO tumors demonstrated rescue of oxidative stress (Figure 3D).

One mechanism by which AMPK could combat ROS is by phosphorylating and inactivating ACC1 and ACC2, thereby shutting down FAS, which is a major consumer of NADPH in the cells. By inhibiting ACC2, AMPK also reverses the inhibition of fatty acid transport into the mitochondria and promotes FAO and, thus, provides an alternate source of NADPH through ME1 and IDH1. Thus, suppressing ACC1 or ACC2 in AMPK-KO cells could decrease ROS levels and restore metastasis. We knocked down either ACC1 or ACC2 in 231LM2 AMPK-KO cells (Figure 3E). We also overexpressed catalase, a ROS-scavenging protein, to decrease ROS levels in 231LM2 AMPK-KO cells (Figure 3F). These cells were subjected to matrix detachment, and knockdown of ACC1 or ACC2 and overexpression of catalase significantly reduced ROS levels comparable to NAC-treated cells (Figure S4F). Importantly, knockdown of ACC1 or ACC2 reduced the NADP/NADPH ratio in AMPK-KO cells during matrix detachment (Figure 4G). We then repeated the orthotopic xenograft experiments with the ACC1- or ACC2-knockdown and catalase-overexpressing cells and found that metastatic ability was restored in the absence of AMPK (Figure 3G). We also measured 4-HNE levels and found that oxidative stress was significantly reduced by ACC1 knockdown and catalase overexpression (Figure 3H). These results provide further support that AMPK-mediated inhibition of ACC1 or ACC2 is required for metastasis and that reducing ROS overcomes the requirement of AMPK for metastasis.

Author Manuscript Author Manuscript Author Manuscript Author Manuscript

AMPK cooperates with CD36 to promote metastasis

The suppression of FAS by inhibition of ACC in response to AMPK activation suggests that cells require a supplement of exogenous fatty acids to maintain their lipid pool. Consistently, we recently showed that induction of the fatty acid transporter CD36 during long-term matrix detachment is dependent on AMPK.[15] We also found that under high-fat diet (HFD) conditions, ectopic expression of CD36 promotes metastasis even in the absence of AMPK.[15] We therefore examined CD36 expression in an MMTV-PyMT mouse model in the absence of AMPK. Although we found expression of CD36 in tumors in PM and PL mice, CD36 expression was diminished when AMPK was deleted in PAM and PAL mice (Figures 4A and 4B). Likewise, the deletion of AMPK in MCF10CA1a tumors reduced the expression of CD36 (Figure 4C). We ectopically expressed CD36 in MCF10CA1a AMPK-KO cells (Figure 4D). The cells were subjected to orthotopic transplantation, and metastasis was quantified. As shown in Figure 4E, the ectopic expression of CD36 in AMPK-KO cells was able to restore metastasis, the same as we previously found in conditions of HFD.[15] Mechanistically, we hypothesized that CD36 could increase FAO[24,25] in the absence of AMPK to regenerate NADPH by ME1 or IDH1 and, therefore, help to combat ROS. Indeed, growth under matrix detachment increased ROS in AMPK-KO cells, which is reduced by ectopic expression of CD36 to the same extent as by treatment with NAC (Figure 4F). Likewise, the NADP/NADPH ratio was increased in AMPK-KO detached cells in comparison to WT detached cells, while the expression of CD36 in AMPK-KO detached cells decreased the NADP/NADPH ratio (Figure 4G). FAO was reduced in detached AMPK-KO cells compared to WT, and the addition of palmitic acid, a long-chain fatty acid used for FAO, does not stimulate FAO in AMPK-deficient cells (Figure 4H). However, the expression of CD36 in AMPK-KO recovered FAO in AMPK-KO detached cells and stimulated FAO in response to palmitate treatment (Figure 4H). Thus, CD36 is sufficient to overcome AMPK deficiency to promote FAO. Finally, ectopic expression of CD36 decreased 4-HNE staining induced by AMPK KO in the primary tumors, demonstrating that CD36 rescues oxidative stress *in vivo* (Figure 4I).

DISCUSSION

Numerous studies had shown that the activation of AMPK could inhibit tumor growth. This was largely attributed to the ability of AMPK to inhibit mTORC1 and protein synthesis. We showed that AMPK activation during energy stress, such as glucose deprivation, prolongs cell survival via redox regulation.[1] Under these conditions, NADPH generation by the PPP is impaired, but AMPK induces alternate routes to maintain NADPH levels and inhibit cell death. Interestingly, during matrix detachment, cells markedly decrease glucose uptake by up to 80% despite glucose availability.[1,8] Alternate routes by which AMPK maintains NADPH homeostasis include inhibition of FAS that consumes NADPH and elevation of FAO through the inhibition of ACC1 and ACC2, respectively. By promoting FAO, AMPK provides acetyl-CoA to drive the TCA cycle, thereby increasing the transport of malate and citrate to the cytosol, the flux from malate to pyruvate by ME1, and the conversion of isocitrate to αKG by IDH1, all of which generate NADPH. Interestingly, FAO can also potentially increase ROS level. However, this ROS level is much lower than ROS generated by pyruvate oxidation,[26] and in fact, FAO inhibits pyruvate oxidation.[27]

Author Manuscript Author Manuscript Author Manuscript Author Manuscript

Over the years, following our initial observation that AMPK is pro-tumorigenic, several publications further established this observation. First, there is evidence that there are no loss-of-function mutations in the genes encoding the subunits of AMPK in cancer. By contrast, the genes encoding for AMPKα1 and AMPKα2 subunits are frequently amplified in human cancer.[28] Others have shown that AMPK is required for tumorigenesis in leukemia and glioblastoma.[9,10] More recently, in a mouse model of NSCLC induced by p53 deletion and the activation of KRAS, it was shown that AMPK depletion inhibits, rather than promotes, tumorigenesis.[11] Moreover, higher levels of pACC1, an AMPK target, was shown to play a pro-metastatic role in breast and lung cancers[12] and pACC1 levels were directly proportional to the node-positive status and worse overall survival in patients with HNSCC and breast cancer.[12,13] However, it is not known if AMPK is required for metastasis, and no genetic evidence has been provided to support that. We propose that, the same as with primary tumor growth, the detached disseminating cells display reduced glucose consumption, energetic stress, and oxidative stress during metastasis.

All our studies consistently demonstrated the requirement of AMPK for metastasis, as its deletion resulted in a marked reduction in metastatic colonization to the lungs. We were able to show that AMPK promoted metastasis by counterbalancing the ROS levels. ROS neutralization by either NAC treatment or the expression of catalase in AMPK-KO cells overcame the requirement of AMPK for metastasis. The loss of either ACC1 or ACC2 was able to reduce oxidative damage that occurred with the loss of AMPK and restored the metastatic potential of the AMPK-KO cells.

Recently we showed that during matrix detachment and under an HFD, AMPK is required for the expression of the fatty acid transporter CD36 and can overcome the requirement of AMPK for metastasis under an HFD.[15] Here, we provided genetic evidence that AMPK is required for CD36 expression in mouse models of breast cancer metastasis. Intriguingly, CD36 overexpression in an AMPK-null background was able to reduce ROS levels during matrix detachment. The reduction of ROS could be because of increased FAO by exogenous fatty acids to drive NADPH production via ME1 and IDH1 activities.[1] Finally, CD36 was able to compensate for AMPK loss in restoring metastasis by counteracting ROS-induced damage. CD36 has been implicated in promoting metastasis under an HFD.[15,16] However, our results suggest that it is also required for the metastasis of breast cancer in the absence of an HFD. One possibility is that the fat tissue in the mammary gland provides auxotrophic fatty acids to compensate for the inhibition of FAS when AMPK is activated. As indicated earlier, it was reported that the knockdown of AMPK in orthotopic breast cancer models inhibited metastasis by preventing pyruvate dehydrogenase complex (PDHc) activation to maintain the TCA cycle.[14] It was reported that AMPK directly phosphorylates and activates the PDHA catalytic subunit to maintain the TCA cycle by supporting the conversion of pyruvate to acetyl-CoA in the mitochondria. However, it is not clear how pyruvate is generated under energetic stress when glucose is not available. It was also reported that by phosphorylating and inhibiting ACC, AMPK activation inhibits ferroptosis.[29] Although we do not have an indication that ferroptosis is induced when we delete AMPK, these results are consistent with our results.

Author Manuscript Author Manuscript Author Manuscript Author Manuscript

In conclusion, our studies provide the first strong genetic evidence for the pro-metastatic role of AMPK. AMPK activation provides an alternate source of NADPH to help overcome the increased ROS levels during metastasis. It does so by shutting down FAS and promoting fatty acid uptake by increasing the expression and membrane translocation of CD36. This combination of AMPK activity and CD36 expression could promote the survival of disseminating tumor cells.

Limitations of the study

Our study focused on the role of AMPK in breast cancer metastasis, and we have not studied extensively the effect of AMPK and its activity on the primary tumors. To eliminate the effect of tumor growth on metastasis, we analyzed the mice at the endpoint where tumor growth is the same in PM and PAM and PL and PAL mice. However, to our surprise, we found that the deletion of AMPK does not affect the time that mice reached the endpoint. It is not clear why we do not see the effect on primary tumor growth in this model. One possibility is that tumor growth in the MMTV-PyMT model is relatively fast, and therefore differences are not apparent. We have not followed the kinetics of metastasis in the MMTV-PyMT mouse models because the spontaneous nature of this model prohibited this type of analysis. We also did not compare the size of the metastatic lesion after AMPK deletion but rather quantified all visible metastatic lesions. Finally, it is expected that the deletion of AMPK would markedly decrease the number of circulating tumor cells, but this was not studied.

RESOURCE AVAILABILITY

Lead contact

Requests for further information and resources should be directed to the lead contact, Nissim Hay (nhay@uic.edu).

Materials availability

All unique/stable reagents generated in this study and listed in the key resources table are available from the lead contact with a completed materials transfer agreement.

Data and code availability

- Additional data reported in this study will be shared by the lead contact upon request.
- This paper does not report any original code.
- Any additional information required to reanalyze the data reported in this study is available from the lead contact upon request.

STAR★METHODS

EXPERIMENTAL MODEL AND STUDY PARTICIPANT DETAILS

Animals: All *in vivo* experiments were performed with prior approval by the Institutional Animal Care and Use Committee at the University of Illinois Chicago. All mice strains,

Author Manuscript Author Manuscript Author Manuscript Author Manuscript

their genotypes and generation have been elaborated above in Reagents and Resources and are in C57Bl6 background. Only female mice were used in the experiments. Once tumors were palpable, around 8–12 weeks of age, the mice were provided Doxycycline in sucrose water (5 mg/ml of D-sucrose) at a concentration of 1 mg/ml. Mice were sacrificed when any tumor endpoint criteria were met. Individual tumors were removed and weighed, some samples were flash frozen and stored at −80, while others were fixed in formalin. Lungs were inflated with PBS, removed, and macrometastases were counted. Lungs were fixed in formalin, and micrometastases were quantified after paraffin embedding and H&E staining. Orthotopic implantations were done in NSG mice as before.[15] All mice for a given experiment were sacrificed when the first mouse reached tumor endpoint criteria. Individual tumors were removed and weighed, some samples were flash frozen and stored at −80, while others were fixed in formalin. Lungs were inflated with PBS, removed, and macrometastases were counted. Lungs were fixed in formalin, and micrometastases were quantified after paraffin embedding and H&E staining. For NAC treatment, NAC was provided in the water at a concentration of 1 mg/ml after the occurrence of palpable tumors in PM/PAM mice around 8–12 weeks of age. Metastasis load was assessed at the endpoint as before.[15]

Cell culture: MDA-MB-231 cells (all clones) and E0771 cells were a kind gift from Dr. Emrah Er (UIC). 293FT cells were acquired from ThermoFisher. Phoenix-AMPHO cells were acquired from ATCC. MCF10CA1a cells were a gift from Dr. Ajay Rana (UIC). MDA-MB-231, 293FT, Phoenix-AMPHO, and E0771 cells were cultured in DMEM (Corning 10–017-CV), supplemented with 10% FBS (Gemini) and 1% penicillin/streptomycin (Corning 30–002-CI). MCF10CA1a cells were cultured in DMEM/F12 (10–090-CMR) supplemented with 5% horse serum (ThermoFisher), 20 ng/mL EGF (Peprotech), 0.5 mg/ml hydrocortisone (Sigma), 100 ng/ml Cholera Toxin (Sigma), 10μg/ml insulin (Sigma), and 1% penicillin/streptomycin (Corning 30–002-CI).

METHOD DETAILS

Cloning and plasmids: pBabe empty vector with hygromycin resistance were gifted from Hartmut Land & Jay Morgenstern & Bob Weinberg[31] (Addgene #1764). pBabe CD36 was generated previously.[15] sgRNAs were cloned into LentiCRISPRv2 puro (Addgene #52961, gift from Feng Zhang[32]) according to the recommended protocol on Addgene's webpage. sgRNAs were designed on CRISPOR.tefor.net or generated previously as noted. pLNCX2 empty vector and pLNCX2 catalase KANL was a gift from Dr. Zachary Schafer (Notre Dame). Human shRNA targeting ACC1 and ACC2 were generated previously.[1]

CRISPR-Cas9 deletion of AMPK: MDA-MB-231 AMPKα1/α2 double knock out cell lines were generated as previously described.[15] Briefly, cells were transfected with LentiCRISPRv.2 sgAMPKα1/α2 in lipofectamine 2000. 24h later, cells were selected with puromycin for 72h. Surviving cells were then plated by limiting dilution for colony selection. Clones were selected and screened for AMPK-deficiency by western blot, and 3–5 clones were expanded and pooled together for generation of the cell line and further experiments. The MCF10CA1a AMPKα1/α2 double knock out cells were generated previously.[15] EO771 cells AMPKα1/α2 double knockout cells were transduced with one

Author Manuscript Author Manuscript Author Manuscript Author Manuscript

of three unique LentiCRISPRv.2 sgAMPKα1/α2 lentiviruses that each target both AMPK a1 and a2, and LentiCRISPRv.2 empty vector was used as a control.

Lentivirus and retrovirus production, transduction, and antibiotic selection: For lentivirus production, 293FT cells were reverse transfected onto poly-L-lysine (sigma) coated 10cm plates. 9μg of Virapower packing mix (ThermoFisher K497500) and 3μg of lentiviral plasmid was packaged in 36μL of Liptofectamine 2000 in 3mL of optiMEM. 16h after transfection, media was aspirated and 6mL of complete media was added. 24h later, media was collected in 6mL of complete media was added. 24h later, media was collected and pooled for a total of 12mL. Viral supernatant was centrifuged at 500g for 5 min, filtered through a 0.45μm filter (Millipore).

For retrovirus production, Phoenix-AMPHO cells were transfected at 70–80% confluency on a 10cm plate. 12μg of pBabe plasmid with 6μg of VSV-G (Addgene #8454, gifted from Bob Weinberg[33]) were packaged in 60μl of Lipofectamine 2000 (Thermo Fisher) in 3mL of optiMEM (Thermo Fisher) with 10mL of complete media. 16h after transfection, media was aspirated and 10mL of complete media was added. 48h later, media was collected, centrifuged at 500g for 5 min, and filtered through a 0.45μm filter (Millipore). Cells were transduced on 10cm plates at 40–50% confluence. 2–4mL of viral supernatant was diluted in 2–4mL of complete media, for a total of 6mL, with 1 mg/ml polybrene (sigma). Transduction was done overnight. The next morning, media was refreshed. 24h later, antibiotics were added. Puromycin was used at 1 mg/ml, blasticidin at 10 mg/ml. An untransduced negative control plate was used to determine when selection was done. Cells were always passaged one additional time in antibiotics to ensure full selection (usually 4–6 days for puromycin and 6–8 days for blasticidin), before expansion and freezing of 10–15 vials.

Matrix detachment experiments: 10g of poly-HEMA (Sigma P3932) was dissolved in 500mL 95% EtOH overnight on a shaker at 37°C. 6-well (2mL/well) plates were coated with poly-HEMA overnight in a closed tissue culture hood with the blower off. Afterward the plates were exposed to UV light for 30-min prior to use. Cells were plated at a density of 0.3×10^6 cells/well on a 6-well plates and 1,000 cells in 100μl were plated on 96-well plates. Bright field images were acquired on a Celigo Live Cell Imager. Matched attached control samples were plated on same size plates at same density and volume of detached samples. For western blot, each sample was an aggregate of 2–3 wells pooled together to control for variability between wells, washed 1x with PBS, and resuspended in PBS and cell pellets were stored at −80°C until lysis.

Western blots: Cell pellets were resuspended in 1x RIPA buffer (CST #9806) supplemented with a protease inhibitor tablet (ThermoFisher A32963) and a phosphatase inhibitor tablet (A32957). Samples were vortexed on top speed for 10 s every 10 min for a total of 30 min. Lysates were centrifuged at 13,000g for 10 min at 4°C to remove debris. The supernatant was moved to a fresh tube, and protein concentration was determined by Bio-Rad protein assay kit (#5000006). 30μg of protein was ran on Bio-Rad TGX gradient gels, either 4%–15% or 4%–20%. Protein was transferred onto PVDF membrane at 115V for 90 min at 4°C. After transfer, membranes were dried. After re-activation, membranes

Author Manuscript Author Manuscript Author Manuscript Author Manuscript

were stained with ponceau (Sigma P7170) for 1 min, washed 3x in dH_2O. Membranes were blocked for 30 min in 5% milk (catalog) dissolved in TBS supplemented with 0.1% Tween (ThermoFisher #003005) (TBS-T). CD36 membranes were blocked in BSA, because milk contains CD36 antigens. Primary antibodies incubation was done in 2.5% BSA in TBS-T. Membranes were sealed in individual, heat-sealed bags over night on a rocker at 4°C. The next day, membranes were washed 3x with TBS-T, and secondary antibody incubation was done in 2.5% milk at RT for 60–90 min on a rocker. Membranes were washed 3x in TBS-T and developed using an Azure cSeries. Western blot quantification was performed using ImageStudio software (Licor).

ROS quantification: ROS levels were quantified by adding a 10X solution of CM-H2DCFDA and Hoechst for a final concentration of 5μM of DCF-DA and 10μg/ml Hoechst, and cells were incubated for 60 min at 37°C. When incubation time is over, plate was centrifuged at 800rpm for 5min and 80% of incubation volume was removed and replaced by PBS. Plate was then imaged on a Celigo live cell imager, and ROS were expressed as the DCF average Integrated Intensity corrected by the total number of cells (Hoechst count).

Tissue staining and immunohistochemistry: Breast tumor tissues were freshly collected and directly fixed in 10% formalin (Fisher Chemical). The lungs were inflated with PBS via the trachea and then removed from the ribcage, washed in PBS and dissected to lobules, before fixing in 10% formalin. After fixation for 24–48 h (depending on tissue size) in formalin, the tissues were processed and embedded in paraffin blocks. The sections (5 μm) were stained with hematoxylin and eosin (H&E). For immunohistochemistry, antigen retrieval was performed by incubating the sections in 0.01 M sodium citrate (pH 6.0) at 95°C for 20 min, followed by cooling down to room temperature. The sections were treated with 3% H_2O_2 in water for 10 min to quench endogenous hydrogen peroxide. After blocking with normal serum, the sections were incubated with primary antibody at 4°C overnight. After incubation with the appropriate secondary antibodies from Vectastain ImmPress Kits (Vector Labs), a 3, 3 -diaminobenzidine (DAB) kit (Vector Labs) was applied to visualize the signal. The sections were then lightly counterstained with hematoxylin. To determine the lung metastatic incidence metastatic nodules were counted under the microscope after H&E staining. Pictures of 4 random fields were taken from each lung section and quantification was performed as per the pathologist scoring criteria.[22]

Seahorse FAO assay: Assay was conducted according to Seahorse protocol, with slight modification. Cells were grown in detached condition for 96h (media change at 48h). Suspension cells were then collected by allowing cells to pellet softly on their own, washed two times with PBS, and media was replaced with substrate limitation media (DMEM supplemented with 0.5 mM glucose, 1 mM glutamine, 1% dialyzed FBS and mM L carnitine) for 24h. For Seahorse FAO assay, suspension cells were collected, washed twice with PBS, dissociated with trypsin at 37°C. Thirty thousand cells per well were then plated in recommended Seahorse FAO buffer on a Seahorse poly-L-lysine coated plate. The plate was centrifuged for 5 min at 800 rpm and transferred into a CO2-free incubator for 4h in presence of BSA or Palmitate-BSA. Measurements were then performed as described in the

Author Manuscript Author Manuscript Author Manuscript Author Manuscript

manufacturer's protocol. Values were normalized to cell number as determined by Hoechst staining on a Celigo live cell imager.

NADP/NADPH ratio: Cells were grown in detached conditions on 6-well plates for 96h (media changed at 48h). Cells in suspension were then collected, centrifuged at 4°C, and rinsed twice with ice-cold PBS. Samples were then treated according to NADP+/NADPH-Glo assay kit manufacturer's protocol (Promega).

QUANTIFICATION AND STATISTICAL ANALYSIS

When comparing two groups, a student two-sided T test was performed. When comparing more than two groups, ANOVA was used. All statistical analysis was performed in PRISM. Statistical method used and sample size (n) is indicated in legends for each figure.

Supplementary Material

Refer to Web version on PubMed Central for supplementary material.

ACKNOWLEDGMENTS

N.H. acknowledges support from the VA Merit Award BX005092, the VA Research Career Scientist Award IK6BX004602, and NIH grants R01AG016927, R01CA090764, R01CA206167, and R01CA258299.

REFERENCES

1. Jeon SM, Chandel NS, and Hay N. (2012). AMPK regulates NADPH homeostasis to promote tumour cell survival during energy stress. Nature 485, 661–665. 10.1038/nature11066. [PubMed: 22660331]
2. Piskounova E, Agathocleous M, Murphy MM, Hu Z, Huddlestun SE, Zhao Z, Leitch AM, Johnson TM, DeBerardinis RJ, and Morrison SJ (2015). Oxidative stress inhibits distant metastasis by human melanoma cells. Nature 527, 186–191. 10.1038/nature15726. [PubMed: 26466563]
3. Le Gal K, Ibrahim MX, Wiel C, Sayin VI, Akula MK, Karlsson C, Dalin MG, Akyu€rek LM, Lindahl P, Nilsson J, and Bergo MO (2015). Antioxidants can increase melanoma metastasis in mice. Sci. Transl. Med 7, 308re8. 10.1126/scitranslmed.aad3740.
4. TeSlaa T, Ralser M, Fan J, and Rabinowitz JD (2023). The pentose phosphate pathway in health and disease. Nat. Metab 5, 1275–1289. 10.1038/s42255-023-00863-2. [PubMed: 37612403]
5. Hay N. (2021). How to inhibit breast cancer and breast cancer metastasis with Akt inhibitors: Lessons learned from studies in mice. J. Breast Cancer Res 1, 30–33. [PubMed: 35578699]
6. Patra KC, and Hay N. (2014). The pentose phosphate pathway and cancer. Trends Biochem. Sci 39, 347–354. 10.1016/j.tibs.2014.06.005. [PubMed: 25037503]
7. Schafer ZT, Grassian AR, Song L, Jiang Z, Gerhart-Hines Z, Irie HY, Gao S, Puigserver P, and Brugge JS (2009). Antioxidant and oncogene rescue of metabolic defects caused by loss of matrix attachment. Nature 461, 109–113. 10.1038/nature08268. [PubMed: 19693011]
8. Parker SJ, Svensson RU, Divakaruni AS, Lefebvre AE, Murphy AN, Shaw RJ, and Metallo CM (2017). LKB1 promotes metabolic flexibility in response to energy stress. Metab. Eng 43, 208–217. 10.1016/j.ymben.2016.12.010. [PubMed: 28034771]
9. Saito Y, Chapple RH, Lin A, Kitano A, and Nakada D. (2015). AMPK Protects Leukemia-Initiating Cells in Myeloid Leukemias from Metabolic Stress in the Bone Marrow. Cell Stem Cell 17, 585–596. 10.1016/j.stem.2015.08.019. [PubMed: 26440282]
10. Chhipa RR, Fan Q, Anderson J, Muraleedharan R, Huang Y, Ciraolo G, Chen X, Waclaw R, Chow LM, Khuchua Z, et al. (2018). AMP kinase promotes glioblastoma bioenergetics and tumour growth. Nat. Cell Biol 20, 823–835. 10.1038/s41556-018-0126-z. [PubMed: 29915361]

Author Manuscript Author Manuscript Author Manuscript Author Manuscript

11. Eichner LJ, Brun SN, Herzig S, Young NP, Curtis SD, Shackel-ford DB, Shokhirev MN, Leblanc M, Vera LI, Hutchins A, et al. (2019). Genetic Analysis Reveals AMPK Is Required to Support Tumor Growth in Murine Kras-Dependent Lung Cancer Models. Cell Metab. 29, 285–302.e7. 10.1016/j.cmet.2018.10.005. [PubMed: 30415923]
12. Rios Garcia M, Steinbauer B, Srivastava K, Singhal M, Mattijssen F, Maida A, Christian S, Hess-Stumpp H, Augustin HG, Mu€ller-Decker K, et al. (2017). Acetyl-CoA Carboxylase 1-Dependent Protein Acetylation Controls Breast Cancer Metastasis and Recurrence. Cell Metab. 26, 842–855.e5. 10.1016/j.cmet.2017.09.018. [PubMed: 29056512]
13. Su YW, Lin YH, Pai MH, Lo AC, Lee YC, Fang IC, Lin J, Hsieh RK, Chang YF, and Chen CL (2014). Association between phosphorylated AMP-activated protein kinase and acetyl-CoA carboxylase expression and outcome in patients with squamous cell carcinoma of the head and neck. PLoS One 9, e96183. 10.1371/journal.pone.0096183. [PubMed: 24769813]
14. Cai Z, Li CF, Han F, Liu C, Zhang A, Hsu CC, Peng D, Zhang X, Jin G, Rezaeian AH, et al. (2020). Phosphorylation of PDHA by AMPK Drives TCA Cycle to Promote Cancer Metastasis. Mol. Cell 80, 263–278.e7. 10.1016/j.molcel.2020.09.018. [PubMed: 33022274]
15. Terry AR, Nogueira V, Rho H, Ramakrishnan G, Li J, Kang S, Pathmasiri KC, Bhat SA, Jiang L, Kuchay S, et al. (2023). CD36 maintains lipid homeostasis via selective uptake of monounsaturated fatty acids during matrix detachment and tumor progression. Cell Metab. 35, 2060–2076.e9. 10.1016/j.cmet.2023.09.012. [PubMed: 37852255]
16. Pascual G, Avgustinova A, Mejetta S, Martín M, Castellanos A, Attolini CSO, Berenguer A, Prats N, Toll A, Hueto JA, et al. (2017). Targeting metastasis-initiating cells through the fatty acid receptor CD36. Nature 541, 41–45. 10.1038/nature20791. [PubMed: 27974793]
17. Hay N. (2016). Reprogramming glucose metabolism in cancer: can it be exploited for cancer therapy? Nat. Rev. Cancer 16, 635–649. 10.1038/nrc.2016.77. [PubMed: 27634447]
18. Gyorffy B. (2021). Survival analysis across the entire transcriptome identifies biomarkers with the highest prognostic power in breast cancer. Comput. Struct. Biotechnol. J 19, 4101–4109. 10.1016/j.csbj.2021.07.014. [PubMed: 34527184]
19. Osz A, Lanczky A, and Gyorffy B. (2021). Survival analysis in breast cancer using proteomic data from four independent datasets. Sci. Rep 11, 16787. 10.1038/s41598-021-96340-5. [PubMed: 34408238]
20. Maglione JE, Moghanaki D, Young LJ, Manner CK, Ellies LG, Joseph SO, Nicholson B, Cardiff RD, and MacLeod CL (2001). Transgenic Polyoma middle-T mice model premalignant mammary disease. Cancer Res. 61, 8298–8305. [PubMed: 11719463]
21. Nakada D, Saunders TL, and Morrison SJ (2010). Lkb1 regulates cell cycle and energy metabolism in haematopoietic stem cells. Nature 468, 653–658. 10.1038/nature09571. [PubMed: 21124450]
22. Chlipala EA, Bendzinski CM, Dorner C, Sartan R, Copeland K, Pearce R, Doherty F, and Bolon B. (2020). An Image Analysis Solution For Quantification and Determination of Immunohistochemistry Staining Reproducibility. Appl. Immunohistochem. Mol. Morphol 28, 428–436. 10.1097/PAI.0000000000000776. [PubMed: 31082827]
23. Shoeb M, Ansari NH, Srivastava SK, and Ramana KV (2014). 4-Hydroxynonenal in the pathogenesis and progression of human diseases. Curr. Med. Chem 21, 230–237. 10.2174/09298673113209990181. [PubMed: 23848536]
24. Abe I, Oguri Y, Verkerke ARP, Monteiro LB, Knuth CM, Auger C, Qiu Y, Westcott GP, Cinti S, Shinoda K, et al. (2022). Lipolysis-derived linoleic acid drives beige fat progenitor cell proliferation. Dev. Cell 57, 2623–2637.e8. 10.1016/j.devcel.2022.11.007. [PubMed: 36473459]
25. Maryanovich M, and Ito K. (2022). CD36-Mediated Fatty Acid Oxidation in Hematopoietic Stem Cells Is a Novel Mechanism of Emergency Hematopoiesis in Response to Infection. Immunometabolism 4, e220008. 10.20900/immunometab20220008. [PubMed: 35465142]
26. Schonfeld P, Wieckowski MR, Lebiedzinska M, and Wojtczak L. (2010). Mitochondrial fatty acid oxidation and oxidative stress: lack of reverse electron transfer-associated production of reactive oxygen species. Biochim. Biophys. Acta 1797, 929–938. 10.1016/j.bbabio.2010.01.010. [PubMed: 20085746]
27. Pettersen IKN, Tusubira D, Ashrafi H, Dyrstad SE, Hansen L, Liu XZ, Nilsson LIH, Løvsletten NG, Berge K, Wergedahl H, et al. (2019). Upregulated PDK4 expression is a sensitive marker of

Author Manuscript Author Manuscript Author Manuscript Author Manuscript

increased fatty acid oxidation. Mitochondrion 49, 97–110. 10.1016/j.mito.2019.07.009. [PubMed: 31351920]

28. Monteverde T, Muthalagu N, Port J, and Murphy DJ (2015). Evidence of cancer-promoting roles for AMPK and related kinases. FEBS J. 282, 4658–4671. 10.1111/febs.13534. [PubMed: 26426570]
29. Lee H, Zandkarimi F, Zhang Y, Meena JK, Kim J, Zhuang L, Tyagi S, Ma L, Westbrook TF, Steinberg GR, et al. (2020). Energy-stress-mediated AMPK activation inhibits ferroptosis. Nat. Cell Biol 22, 225–234. 10.1038/s41556-020-0461-8. [PubMed: 32029897]
30. Chen X, Ariss MM, Ramakrishnan G, Nogueira V, Blaha C, Putzbach W, Islam ABMMK, Frolov MV, and Hay N. (2020). Cell-Autonomous versus Systemic Akt Isoform Deletions Uncovered New Roles for Akt1 and Akt2 in Breast Cancer. Mol. Cell 80, 87–101.e5. 10.1016/j.molcel.2020.08.017. [PubMed: 32931746]
31. Morgenstern JP, and Land H. (1990). Advanced mammalian gene transfer: high titre retroviral vectors with multiple drug selection markers and a complementary helper-free packaging cell line. Nucleic Acids Res. 18, 3587–3596. 10.1093/nar/18.12.3587. [PubMed: 2194165]
32. Sanjana NE, Shalem O, and Zhang F. (2014). Improved vectors and genome-wide libraries for CRISPR screening. Nat. Methods 11, 783–784. 10.1038/nmeth.3047. [PubMed: 25075903]
33. Stewart SA, Dykxhoorn DM, Palliser D, Mizuno H, Yu EY, An DS, Sabatini DM, Chen ISY, Hahn WC, Sharp PA, et al. (2003). Lentivirus-delivered stable gene silencing by RNAi in primary cells. RNA 9, 493–501. 10.1261/rna.2192803. [PubMed: 12649500]

Author Manuscript Author Manuscript Author Manuscript Author Manuscript

Highlights

- AMPK activation is required to mitigate reactive oxygen species levels to support metastasis
- AMPK activation inhibits fatty acid synthesis (FAS) to decrease NADPH consumption
- AMPK supports fatty acid oxidation (FAO) to generate NADPH via malate conversion to pyruvate
- AMPK activation induces CD36 expression to increase fatty acid (FA) uptake and support FAO

Author Manuscript Author Manuscript Author Manuscript Author Manuscript

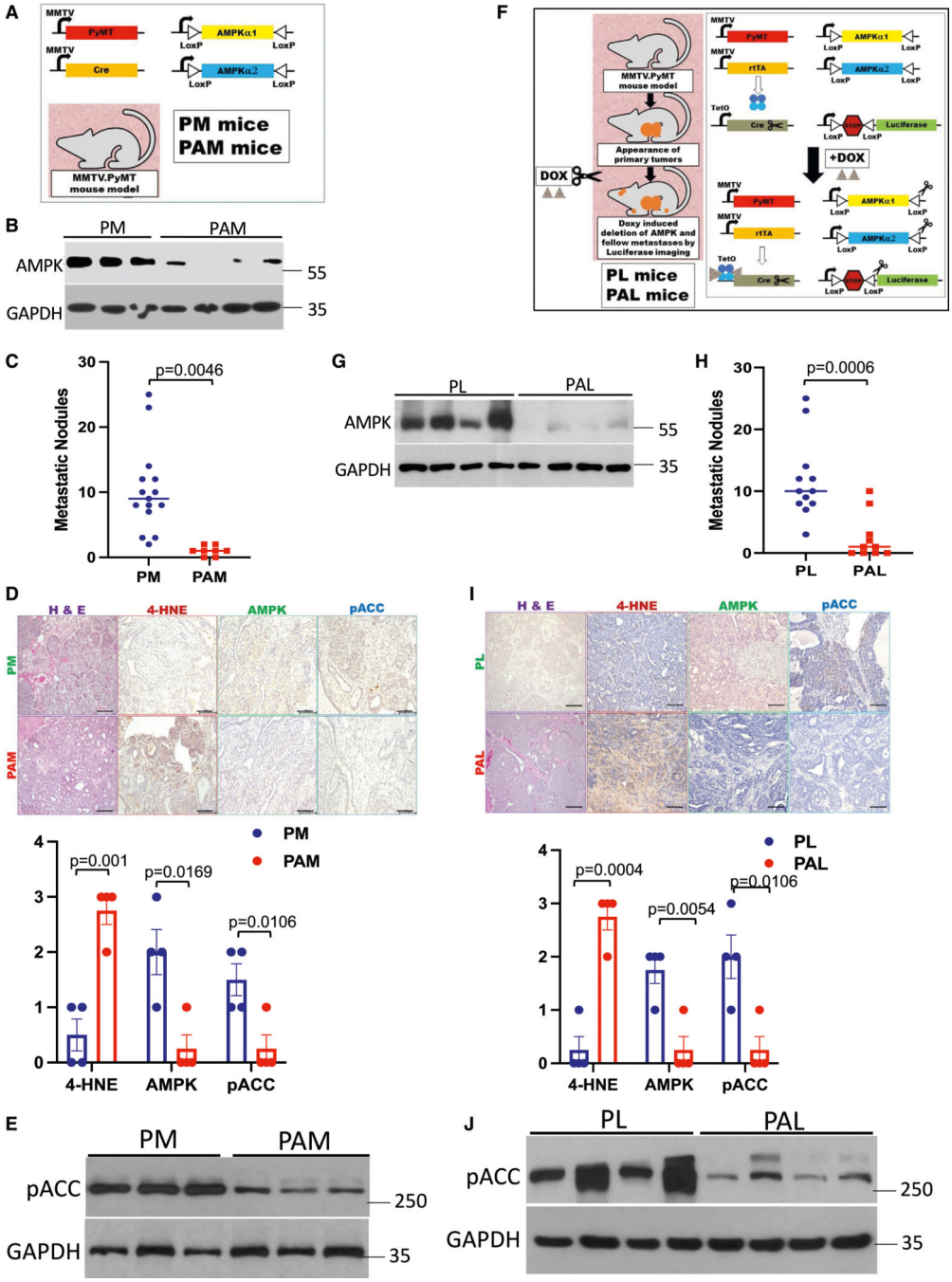

Figure 1. AMPK is required for metastasis in mouse models of breast cancer metastasis

A) Schematic models and genotypes of PM/PAM mice.

(B) Western blotting of tumor tissue from PM and PAM mice for total AMPK (antibody recognizes both α1 and α2).

(C) Quantification of lung metastases in PM and PAM mice (PM = 14 and PAM = 8).

(D) IHC for 4-HNE, AMPK, and pACC on the tumor tissues from PM and PAM mice (top) and quantification (bottom).

(E) Western blotting of tumor tissues from PM and PAM mice for pACC.

Author Manuscript Author Manuscript Author Manuscript Author Manuscript

(F) Schematic models and genotypes of PL/PAL mice.
(G) Western blotting of tumor tissue from PL and PAL mice for total AMPK.
(H) Quantification of lung metastases in the lungs of PL and PAL mice (PL = 12 and PAL = 9).
(I) IHC staining for 4-HNE, AMPK, and pACC on the tumor tissues from PL and PAL mice (left) and quantification (right).
(J) Western blotting of tumor tissues from PL and PAL mice for pACC. All data are presented as the mean ± SEM. A two-tailed t test was used for comparison. Sample size is 4 unless noted differently above.

Author Manuscript
Author Manuscript
Author Manuscript
Author Manuscript

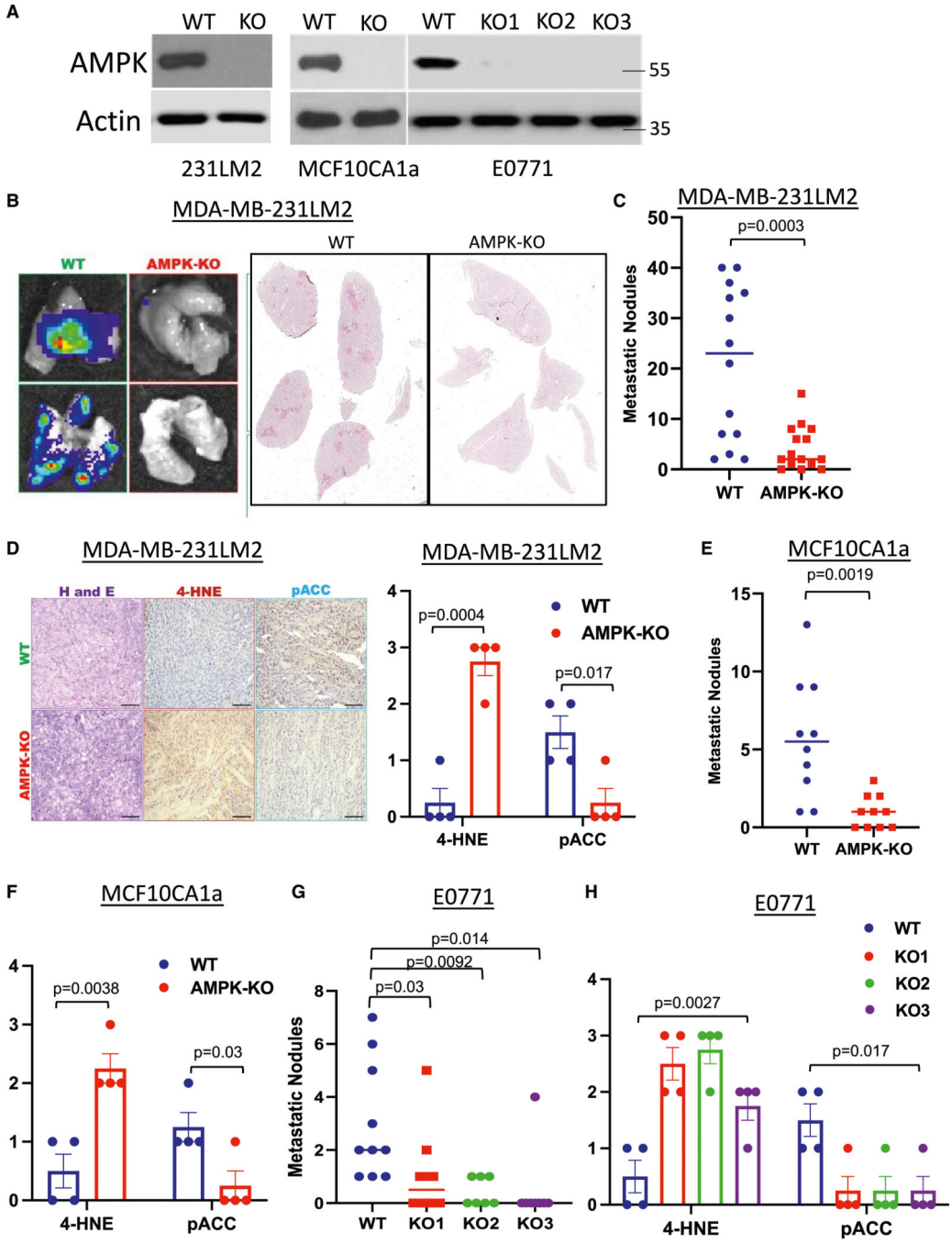

Figure 2. AMPK knockout in metastatic breast cancer cell lines reduced metastasis after orthotopic implantation

(A) Western blots of AMPK in MDA-MB-231LM2, MCF10CA1a, and E0771 cells.

(B) Representative picture of bioluminescent imagining and H&E-stained sections of lungs of NSG mice after orthotopic implantation of 231LM2 WT and AMPK-KO cells.

(C) Quantification of lung metastases in NSG mice after orthotopic implantation of 231LM2 WT and AMPK-KO cells (WT = 14 and AMPK-KO = 15).

(D) IHC for 4-HNE and pACC on the tumor tissues from 231LM2 WT and AMPK-KO cells orthotopically implanted mice (left) and quantification (right).

Author Manuscript Author Manuscript Author Manuscript Author Manuscript

(E) Quantification of metastatic incidence in the lungs of NSG mice after orthotopic implantation of MCF10CA1a WT and AMPK-KO cells (WT = 10 and AMPK-KO = 10).
(F) Quantification of IHC for 4-HNE and pACC on the tumor tissues from MCF10CA1a WT and AMPK-KO cells orthotopically implanted in mice.
(G) Quantification of lung metastases in C57BL/6 mice after orthotopic implantation of E0771 WT and AMPK-KO (KO1, KO2, KO3) cells (WT = 10, KO1 = 10, KO2 = 7, KO3 = 8).
(H) Quantification of IHC for 4-HNE and pACC on the tumor tissues from WT, KO1, KO2, and KO3 E077 cells orthotopically implanted in mice.
All data are presented as the mean ± SEM. For comparison: a two-tailed t test was used in (C)–(G) and one-way ANOVA in (H). Sample size is 4 unless noted differently above.

Author Manuscript
Author Manuscript
Author Manuscript
Author Manuscript

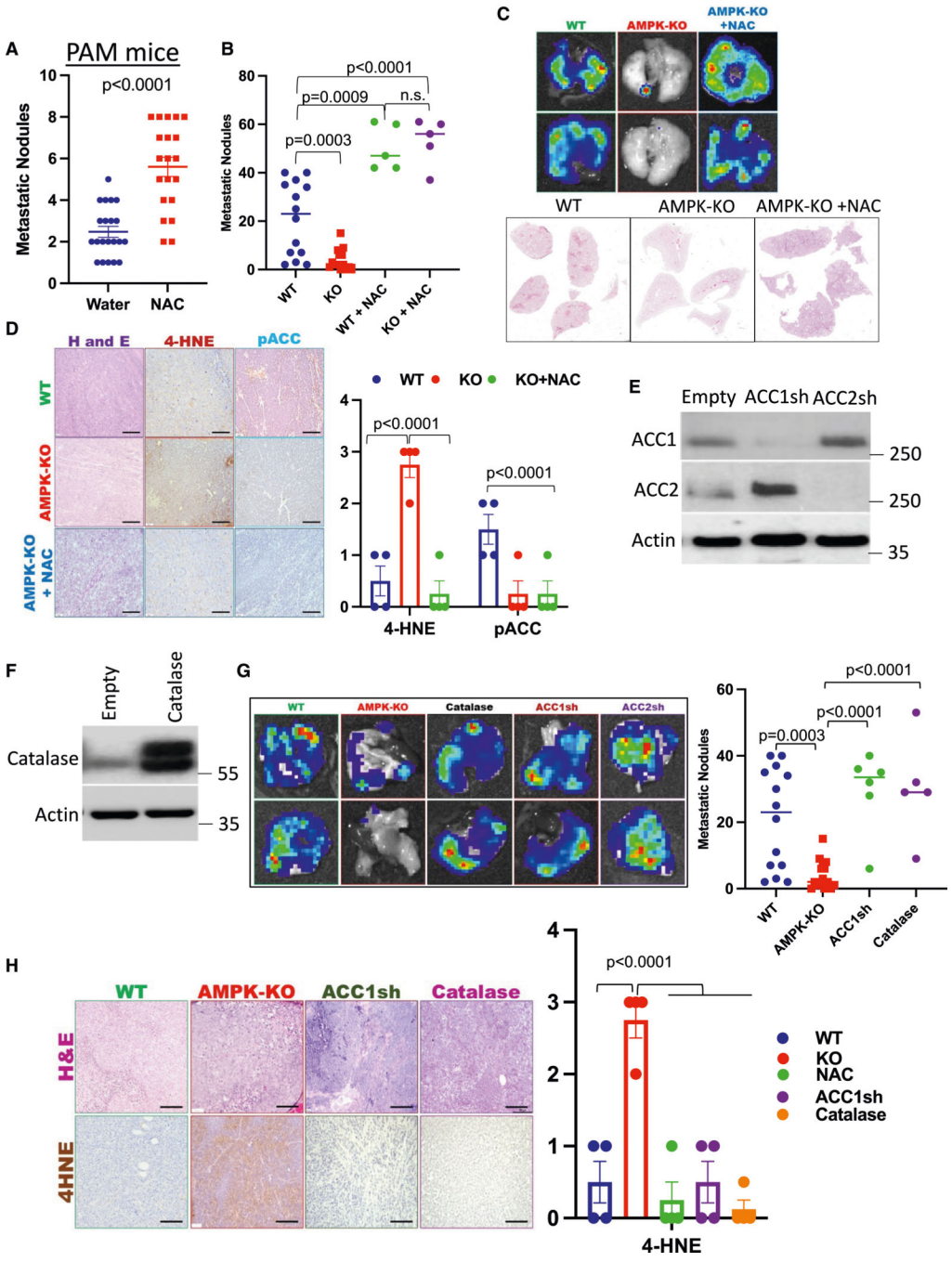

Figure 3. NAC, catalase, and ACC knockdown reverse oxidative stress in AMPK-null cells and restore metastatic potential

(A) Quantification of lung metastases in PAM mice ± NAC administration ($n = 21$).

(B) Quantification of lung metastases in NSG mice after orthotopic implantation of 231LM2 WT and AMPK-KO cells ± NAC treatment (WT = 14, AMPK-KO = 15, WT + NAC = 5, KO + NAC = 5).

(C) Representative picture of bioluminescent imagining (top) and H&E-stained sections (bottom) of lungs from three experimental conditions of (B).

Author Manuscript Author Manuscript Author Manuscript Author Manuscript

(D) Left: representative picture of IHC staining for 4-HNE and pACC on the tumor sections from 231LM2 WT and AMPK-KO tumors and from AMPK-KO tumors treated with NAC. Right: quantification of tumor samples of 4-HNE and pACC staining in tumor sample sections.
(E) Western blot showing ACC1 and ACC2 knockdown in 231LM2 AMPK-KO cells.
(F) Western blot showing catalase overexpression in 231LM2 AMPK-KO cells.
(G) Representative picture of bioluminescent imagining (left) and quantification of metastatic incidence (right) in the lungs of NSG mice after orthotopic implantation of 231LM2;AMPK-KO;ACC1KD, 231LM2;AMPK-KO;ACC2KD, or 231LM2;AMPK-KO catalase-overexpressing cells (WT = 14, AMPK-KO = 15, ACC1 = 6 and catalase = 5). Results are the mean ± SEM using a two-tailed t test.
(H) IHC staining for 4-HNE and pACC on the tumor sample sections from four experimental animals. IHC results are the mean using ordinary one-way ANOVA.
All data are presented as the mean ± SEM. For comparison: a two-tailed t test was used in (C)–(G) and one-way ANOVA in (H). Sample size is 4 unless noted differently above.

Author Manuscript Author Manuscript Author Manuscript Author Manuscript

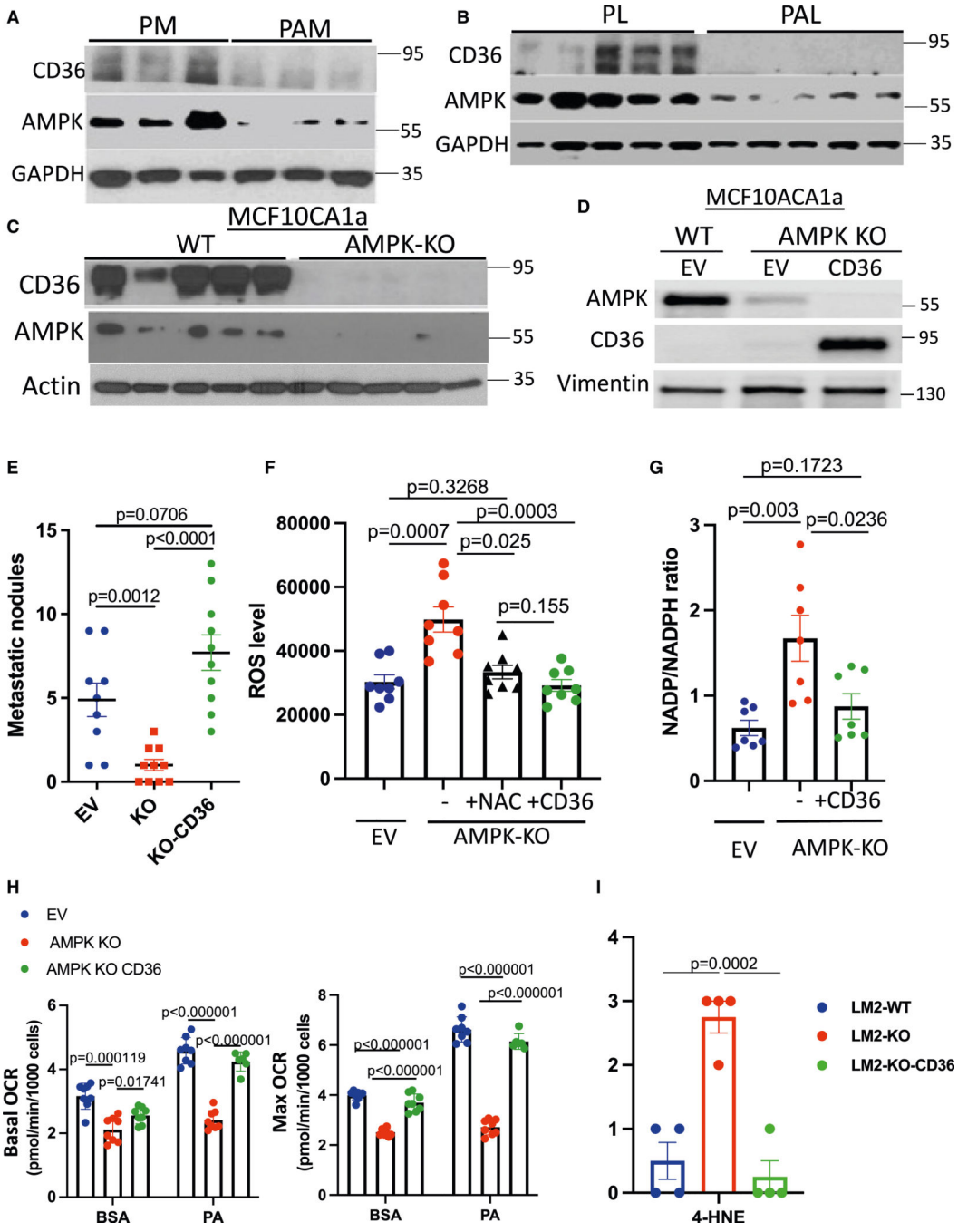

Figure 4. CD36 expression is dependent on AMPK, and its ectopic expression reverses oxidative damage in AMPK-null cells and restores metastasis

(A and B) Western blots showing expression of CD36 in MMTV-PyMT tumors in the presence or absence of AMPK.

(C) Western blot showing expression of CD36 in MCF10CA1a tumors in the presence or absence of AMPK.

(D) Western blot showing ectopic expression of CD36 in MCF10CA1a cells deficient in AMPK.

Author Manuscript Author Manuscript Author Manuscript Author Manuscript

(E) CD36 ectopic expression in AMPK-null MCF10CA1a cells restores metastasis (WT, n = 10 and AMPK-KO, n = 10). Results are the mean using a two-tailed t test.
(F) Ectopic expression of CD36 in AMPK-null MCF10CA1a cells decreased ROS levels under matrix detachment.
(G) Ectopic expression of CD36 in AMPK-null MCF10CA1a reduced NADP/NADPH ratio under matrix detachment.
(H) MCF10CA1a cells were grown under detachment for 96 h, and FAO was determined by Seahorse assay. Oxygen consumption rates (OCRs) in basal (left) and FCCP (right) conditions were measured in nutrient-limited media supplemented with BSA, assessing ‘‘endogenous FAO,’’ or palmitic acid (PA), assessing ‘‘substrate FAO.’’ In both these configurations, the OCR was increased in AMPK-null MCF10CA1a overexpressing CD36. (F–H) Results are the mean ± SEM of 4 independent experiments in duplicate analyzed with a paired Student t test.
(I) Ectopic expression of CD36 reduced oxidative damage, as measured by 4-HNE staining in AMPK-null MCF10CA1a tumors. IHC staining results are the mean ± SEM of 4 independent experiments using an unpaired t test.

Author Manuscript Author Manuscript Author Manuscript Author Manuscript

KEY RESOURCES TABLE

REAGENT or RESOURCE	SOURCE	IDENTIFIER
Antibodies		
Polyclonal goat anti-CD36 (for mouse)	R&D Systems	Cat. # AF2519; RRID: AB_2228767
Monoclonal rabbit anti-CD36 (clone D8L9T, for human)	Cell Signaling Technology	Cat. # 14347; RRID: AB_2798458
Polyclonal rabbit anti-phospho-ACC	Cell Signaling Technology	Cat. # 3661; RRID: AB_330337
Polyclonal rabbit anti-ACC1	Millipore	Cat. # ABS1068
Polyclonal rabbit anti-ACC1	Cell Signaling Technology	Cat. # 3662; RRID: AB_2219400
ACC2	Cell Signaling Technology	Cat# 8578, RRID:AB_10949898
Monoclonal rabbit anti-phospho-AMPKα (clone 40H9)	Cell Signaling Technology	Cat. # 2535; RRID: AB_331250
Polyclonal rabbit anti-AMPKα	Cell Signaling Technology	Cat. # 2532; RRID: AB_330331
Monoclonal mouse anti-Actin	Sigma-Aldrich	Cat. # A5441; RRID: AB_476744
4-HNE	Abcam	Cat# ab46545, RRID:AB_722490
GAPDH	Cell Signaling Technology	Cat# 5174, RRID:AB_10622025
Catalase	Cell Signaling Technology	Cat# 12980, RRID:AB_2798079
Bacterial and virus strains		
Stbl3 bacteria	Thermo Fisher Scientific	Cat. #C2987
Chemicals, peptides, and recombinant proteins		
Doxycycline	Sigma-Aldrich	Cat. #D9891
DMEM 25mM glucose	Corning	Cat. # 10–017-CV
DMEM/F12	Corning	Cat. # 10–090-CMR
DMEM/F12 w/o glucose	US Biological Life Sciences	Cat # 38210000
10x RIPA Buffer	Cell Signaling Technology	Cat. # 9806
Protease inhibitor tablet	Thermo Fisher Scientific	Cat. # A32963
Phosphatase inhibitor tablet	Thermo Fisher Scientific	Cat. # A32957
PolyHEMA	Sigma-Aldrich	Cat. #P3932
Propidium iodide	Sigma-Aldrich	Cat. #P4170–25MG
PVDF membrane	Bio-Rad	Cat. # 1620177
FastDigest BsmBI & 10X FD-buffer	Thermo Fisher Scientific	Cat. # FD0454
FastAP	Thermo Fisher Scientific	Cat. # EF0651
T4 PNK	New England Biolabs	Cat. #M0201S
Quick Ligase	New England Biolabs	Cat. #M2200S
H2DCFDA	Sigma-Aldrich	Cat. #D6883
N-Acetylcysteine	Sigma-Aldrich	Cat. # A7250
D-Luciferin	Sigma-Aldrich	Cat. #L9504
Critical commercial assays		
Q5 High-Fidelity DNA polymerase	New England Biolabs	Cat. #M0491
Gibson Assembly Cloning Kit	New England Biolabs	Cat. #E5510

Author Manuscript Author Manuscript Author Manuscript Author Manuscript

REAGENT or RESOURCE	SOURCE	IDENTIFIER
Deposited data		
Source data and uncropped western blots	This paper	N/A
Experimental models: Cell lines		
MDA-MB-231 Parental and metastatic clones	Gift from Dr Ekram Emrah	N/A
E0771	Gift from Dr Ekram Emrah	N/A
HEK293FT	Thermo Scientific	R70007
MCF10CA1a (female, malignant human mammary epithelia)	Gift from Dr. Ajay Rana (UIC)	N/A
Phoenix-AMPHO	ATCC	CRL-3213
Experimental models: Organisms/strains		
Mouse C57BL.6: *MMTV-PyMT*	Chen et al.[30]	N/A
Mouse PM: *MMTV.PyMT; MMTV.Cre*	This paper	N/A
Mouse PAM: *MMTV.PyMT; AMPKa1$^{fl/fl}$; AMPKa2$^{fl/fl}$; MMTV.Cre*	This paper	N/A
Mouse C57BL/6-*AMPKa1$^{flox/flox}$*	Jackson Labs	*Prkaa1$^{tm1.1Sjm}$*/J
Mouse: C57BL/6-*AMPKa2$^{flox/flox}$*	Jackson Labs	*Prkaa2$^{tm1.1Sjm}$*/J
Mouse: *MMTV.Cre*	Jackson Labs	Tg(MMTV-cre)4Mam/J
Mouse: *Tet(O)Cre*	Jackson Labs	B6.Cg-Tg(tetO-cre)1Jaw/J
Mouse: *MMTV.rtTA*	Jackson Labs	B6; SJL-Tg(MMTV-rtTA)4–1Jek/J
Mouse: *LSL.Luc*	Jackson Labs	FVB.129S6(B6) *Gt (ROSA)26Sor$^{tm1(Luc)Kael}$*/J
NSG	Taconic	NOG-F NOD.Cg-*Prkdc^{scid}Il2rg^{tm1Sug}*/ JicTac
Oligonucleotides		
Human sgAMPKα1/α2 For: caccGCACGACGGGCGGGTGAAGAT	Terry et al.[15]	N/A
Human sgAMPKα1/α2 Rev: aaacATCTTCACCCGCCCGTCGTGC	Terry et al.[15]	N/A
Mouse sgAMPKα1/α2 #1 For: caccgAGAAGCAGAAGCACGACGGG	This paper	N/A
Mouse sgAMPKα1/α2 #1 Rev: aaacCCCGTCGTGCTTCTGCTTCT	This paper	N/A
Mouse sgAMPKα1/α2 #2 For: caccgCACGACGGGCGGGTGAAGAT	This paper	N/A
Mouse sgAMPKα1/α2 #2 Rev: aaacATCTTCACCCGCCCGTCGTG	This paper	N/A
Mouse sgAMPKα1/α2 #3 For: caccGAAGCAGAAGCACGACGGGC	This paper	N/A
Mouse sgAMPKα1/α2 #3 Rev: aaacGCCCGTCGTGCTTCTGCTTC	This paper	N/A
Recombinant DNA		

Author Manuscript Author Manuscript Author Manuscript Author Manuscript

REAGENT or RESOURCE	SOURCE	IDENTIFIER
pBabe hygro – EV	Gift from Hartmut Land, Jay Morgenstern, and Robert Weinberg	Addgene # 1765
pBabe hygro – CD36	Terry et al.[15]	N/A
LentiCRISPRv2 Puro – EV	Gift from Feng Zhang	Addgene # 52961
LentiCRISPRv2 Puro – human sgAMPKa1/a2	Terry et al.	N/A
pCMV-VSV-G packaging plasmid	Robert Weinberg	Addgene # 8454
ViraPower Lentiviral Packaging Mix	Thermo Fisher	Cat. #K497500
LentiCRISPRv2 Puro – mouse sgAMPKa1/a2 #1	This paper	N/A
LentiCRISPRv2 Puro – mouse sgAMPKa1/a2 #2	This paper	N/A
LentiCRISPRv2 Puro – mouse sgAMPKa1/a2 #2	This paper	N/A
pLNCX2 empty vector	Adgene	N/A
pLNCX2 Catalase KANL	This paper	N/A
Software and algorithms		
Image Studio for western blot analysis	LI-COR	N/A
FlowJo for flow cytometry analysis	FlowJo	N/A
PRISM for statistical analysis	GraphPad	N/A
Other		
Chemiluminescent western blot developer	Azure	cSeries
Flow-cytometer	Beckman Coulter	CytoFLEX S
Live cell imaging	Nexcelom Bioscience	Celigo Imaging Cytometer